Journal of Power Sources 221 (2013) 97–107

Contents lists available at SciVerse ScienceDirect

Journal of Power Sources

journal homepage: www.elsevier.com/locate/jpowsour

Combining high temperature electrochemistry and time of flight secondary ion mass spectrometry: Quasi in situ study of lanthanum strontium chromate manganate electrodes

Marcus Rohnke*, Mareike Falk, Anne-Katrin Huber, Jürgen Janek

Institute for Physical Chemistry, Justus-Liebig-University of Giessen, Heinrich-Buff-Ring 58, 35392 Giessen, Germany

HIGHLIGHTS

- ToF SIMS in situ polarisation experiments of SOFC model electrodes.
- Electrode surface composition changes with applied voltage.
- Electrode surface composition changes already during the sinter process.
- Electrode composition can be switched several times by changing the polarity of the voltage.

ARTICLE INFO

Article history:
Received 3 May 2012
Received in revised form
23 July 2012
Accepted 31 July 2012
Available online 11 August 2012

Keywords:
Time of flight secondary ion mass spectrometry
Electrode polarisation
Solid oxide fuel cell
Lanthanum strontium chromate manganate
Activation
Passivation

ABSTRACT

Time of flight secondary ion mass spectrometry (TOF-SIMS) is a well-established technique for the chemical surface and depth analysis of inorganic functional materials. Here we report in detail on the changes in the surface composition of a solid oxide fuel cell (SOFC) thin film model electrode, namely lanthanum strontium chromate manganate (LSCrM, $La_{0.64}Sr_{0.36}Cr_{0.68}Mn_{0.35}O_{3-\delta}$), on yttria stabilised zirconia (YSZ) as solid electrolyte, upon electrochemical polarisation. The electrochemical experiments were performed in the TOF-SIMS analysis chamber allowing fast analysis directly afterwards. Changes in the electrode surface composition occur already after sample annealing in air, i.e. strontium and lanthanum diffuse to the top of the LSCrM electrode and onto the free YSZ surface. By applying either a cathodic or an anodic potential to the electrode, enrichment or depletion of the different cation constituents on both the LSCrM and free YSZ surface were observed. These redistribution phenomena are partly reversible several times upon switching the electrical potential of the LSCrM electrode.

1. Introduction

Fuel cell technology is an attractive method for the conversion of chemical into electrical energy [1,2]. In particular, high temperature solid oxide fuel cells possessing high efficiency and compatibility with different fuels have been developed for more than 30 years. Solid oxide fuel cells (SOFCs) based on zirconia solid electrolyte are not far from serial production, but the high temperature and the corresponding degradation of electrodes during operation continue to pose challenges to current research. Despite serious efforts to introduce intermediate temperature SOFCs, yttria-stabilised zirconia (YSZ) is used primarily as a solid electrolyte, perovskite-type oxide solid solutions are used as cathodes and Ni/YSZ cermets as anodes. Quite a number of experimental studies on the degradation and stability of different electrode systems have been reported [3–7]. The majority either rely on electrical "in situ" characterisation or on ex situ "post mortem" analysis. With recent advances in "in situ" and "in operando" techniques [8–11], a better understanding of electrode reactions and degradation processes can be achieved by a combination of electrochemical and spectroscopic/microscopic experiments with model-type electrodes. To date, the number of systematic attempts in this direction is still small.

From long term investigations on SOFCs it is known that the cell performance deteriorates with time [12]. In the literature this phenomenon is generally explained by degradation effects of either the electrode or the solid electrolyte [13,14]. In particular, a local redistribution of electrode impurities or dopands can be caused either by surface segregation (purely thermodynamic origin) [15] or as a consequence of the applied electrical potential and the resulting atomic fluxes (kinetic demixing, see Ref. [16]). In any case, the

* Corresponding author. Tel.: +49 641 99 34502; fax: +49 641 99 34509.
E-mail address: Marcus.Rohnke@phys.chemie.uni-giessen.de (M. Rohnke).

0378-7753/$ – see front matter © 2012 Elsevier B.V. All rights reserved.
http://dx.doi.org/10.1016/j.jpowsour.2012.07.139

interface and surface composition of the electrodes controls the electrocatalytic activity [17,18], and the observation of the surface composition with high spatial and temporal resolution might provide valuable information on the degradation processes. Unfortunately, the most powerful surface-analytical techniques rely on the use of either electron (photoelectron spectroscopy, electron microscopy) or ion (mass spectrometry, ion scattering) probes, which requires ultra-high vacuum (UHV) conditions. Recently, serious attempts have been undertaken to provide high pressure modifications of these techniques, but the number of reports remains small [8,19]. Here, we report on an intermediate step, employing spatially resolving mass spectrometry as a "quasi" in situ technique. The main purpose of this paper is to show first detailed results and to discuss the performance and the drawbacks of the technique, which to our knowledge has not yet been explored. It is in line with previous studies on the spectroscopic/microscopic analysis of solid state electrodes in operation, i.e. under kinetic load, primarily in the system $Pt(O_2)$/YSZ [20–23] and $Ir(N_2)$YSZ [24], but recently also in perovskite-based cathodes [4,6]. We would like to point out that ex situ SIMS has been applied quite successfully to image fast reaction sites of gas electrodes e.g. by the corresponding spatial distribution of ^{18}O [25,26].

In this paper we present results on lanthanum strontium chromate manganate (LSCrM) electrodes with the nominal composition $La_{0.64}Sr_{0.36}Cr_{0.68}Mn_{0.35}O_{3-\delta}$. LSCrM has recently been proposed as a material for both anodes and cathodes in SOFCs, and it has been claimed that it is also stable under reducing conditions, in contrast to chromium-free LSM (LSM = $La_{1-x}Sr_xMnO_3$) [27]. This would enable symmetric systems to be prepared with LSCrM on both sides of the solid electrolyte.

In the present study we prepared model-type thin film LSCrM electrodes by pulsed laser deposition (PLD) on a single crystalline YSZ solid electrolyte, which were well suited for surface analyses. Within the SIMS chamber we varied $p(O_2)$ and the applied electrical potential V_{WC} to the LSCrM electrode in order to stress the stability of the investigated material. We were then able to follow the surface changes by ToF-SIMS, however, only in an intermittent mode as explained below. For comparison we also performed high pressure ex situ experiments in a conventional furnace under controlled $p(O_2)$.

2. Theoretical background – the defect chemistry of LSCrM

As mentioned in detail in a previous paper [28] the defect chemistry of perovskites is characterised by an oxygen non-stoichiometry, meaning that the perovskite phase can exist with oxygen excess and oxygen deficiency. The stability field at a given cation composition is defined by the thermodynamic variables oxygen partial pressure ($p(O_2)$) and temperature (T). Changes in the oxygen content disturb the material's thermodynamic equilibrium causing various defects in the perovskite material, depending on the oxygen activity. In the oxygen excess range additional oxygen has to be incorporated into the perovskite lattice. The incorporated oxygen can either occupy interstitial sites or the incorporation is accompanied by formation of metal vacancies in one or both sublattices with concomitant oxidation of Mn(III) to Mn(IV) ions. The formation of interstitial sites is only possible under extreme experimental conditions. So for our study we propose the mechanism based on the formation of metal vacancies. The transition to the stoichiometric range is accompanied by elimination of metal vacancies and reduction of Mn(IV) to Mn(III) ions. In the oxygen deficiency range the formation of oxygen vacancies is compensated by partial reduction of Mn(III) to Mn(II) ions.

The starting point of our experiments is the oxygen excess range (Fig. 1a) arising from annealing of the samples in air. Cation vacancies are formed by segregation of these cations (mostly La(III) and Sr(II) ions, due to their higher cation mobility) out of the lattice onto the electrode and electrolyte surface, thus leading to a high surface concentration of La_2O_3 and SrO.

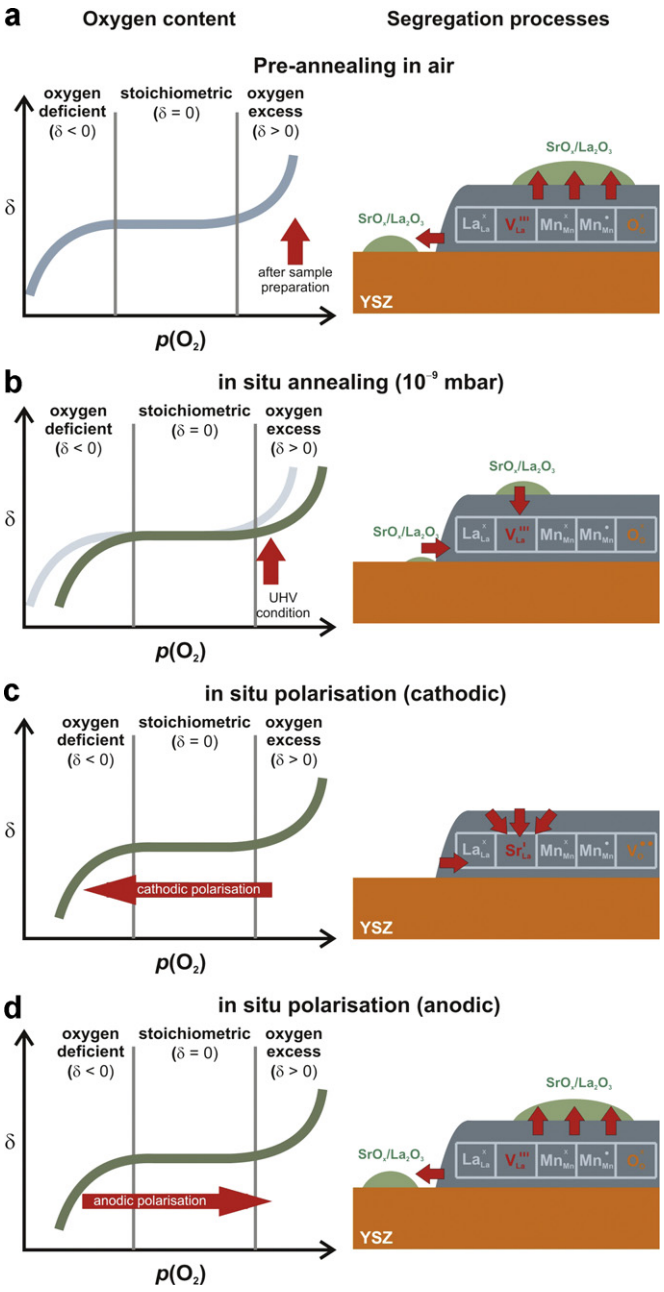

Fig. 1. Schematic diagram of the oxygen stoichiometry of the perovskite phase at different pressures and under electrochemical polarisation and the corresponding defect chemistry.

By reducing the oxygen partial pressure for the UHV experiments ($p(O_2) = 10^{-9}$ mbar–10^{-6} mbar) metal vacancies are consumed. According to studies by Mizusaki [29] with LSM electrodes, we propose that the LSCrM phase is still in the oxygen excess range during our UHV experiments.

In situ annealing inside the SIMS chamber (Fig. 1b) drives the perovskite closer to the stoichiometric range meaning that more metal vacancies are consumed and in conclusion the concentration of La and Sr onto the electrode and electrolyte surface should decrease.

The applied electrical potential V_{WC} influences the oxygen activity locally at the electrode and provides an additional experimental control parameter which disturbs the local equilibrium at the electrode and may cause the local oxygen activity to deviate

from the value fixed at the gas phase. Due to the fact that the in- or ex-corporation of oxygen varies considerably at different locations on the electrode (TPB = triple phase boundary, interface between YSZ and LSCrM and on the LSCrM surface) we have local areas with different oxygen activities and therefore, we may have local differences in the defect chemistry.

By applying a cathodic potential the LSCrM phase is reduced and the material transforms to the oxygen deficiency range (Fig. 1c). This means for the in situ SIMS experiments that a decrease of the surface concentration of La and Sr should be visible due to the consumption of metal vacancies and segregation of both elements back into the perovskite lattice. Reversely, under anodic polarisation the transition in the oxygen excess range occurs and a re-segregation of SrO and La_2O_3 at the electrode and electrolyte surface should be visible (Fig. 1d).

3. Experimental

3.1. Sample preparation and experiments

Thin films of LSCrM were deposited by Pulsed Laser Deposition (PLD) on (111)-orientated YSZ single crystals (9.5 Mol% Y_2O_3 in ZrO_2 (CrysTec, Germany)) with a surface area of 1×1 cm^2 and a thickness between 0.5 mm and 1.0 mm. The deposited LSCrM films had a thickness between 300 nm and 400 nm. The LSCrM target was purchased from HTM Reetz (Berlin, Germany). The composition of the LSCrM target was determined by both inductively coupled plasma optical emission spectrometry (ICP-OES) and energy dispersive X-ray spectroscopy (EDX) to $La_{0.64}Sr_{0.36}Cr_{0.68}Mn_{0.35}O_{3-\delta}$. The PLD was carried out at about 800 °C (temperature of the substrate heater) at an oxygen pressure of about 1×10^{-4} mbar in the PLD chamber. A KrF excimer laser (ComPex LAMBDA Physik Lasertechnik, Göttingen, Germany) was used together with a standard PLD vacuum chamber. The energy and frequency of the laser were 100 mJ per pulse and 10 Hz, respectively. The plasma-exposed surface of the YSZ substrates was covered partly with a stainless steel mask before deposition to prepare a defined three phase boundary between YSZ, LSCrM and the gas phase. After deposition the samples were pre-annealed for 10 h at 1000 °C in air to re-oxidize the LSCrM film (some oxygen is always lost during PLD) and to obtain the homogeneous perovskite phase. The XRD pattern of the LSCrM film together with the theoretical one is shown in Appendix 1 [30]. The intense reflexes between 28° and 31° and between 59° and 63° result from the YSZ substrate.

The backs of the YSZ substrates were painted with platinum paste as counter electrodes, and these were sintered during the annealing procedure. Some samples were cut into two or four pieces to enable their use for different experiments but with the same electrode composition and microstructure. A schematic sketch of the sample geometry is presented in Fig. 2. With the exception of the platinum circle on top of the LSCrM electrode for better electric contact during in situ experiments, the sample setup for in situ and ex situ measurements was identical.

For ex situ annealing experiments the samples were cut into four pieces. One piece was analysed without annealing, the second piece was analysed after 10 h, the third after 30 h and the last one after 100 h annealing at 1000 °C in air. The ex situ polarisation experiments were carried out in a tube furnace. Anode and cathode contacts were made from platinum foil. As voltage sources a Jaissle potentiostat/galvanostat IMP 83 PC and a Keithley 2400 SourceMeter were used. With exception of the first polarisation experiment, all ex situ polarisation experiments were carried out in N_2 atmosphere (5 N) in order to simulate an oxygen activity close to the activity inside the SIMS analysis chamber. The electrode was electrochemically polarised for different lengths of time between

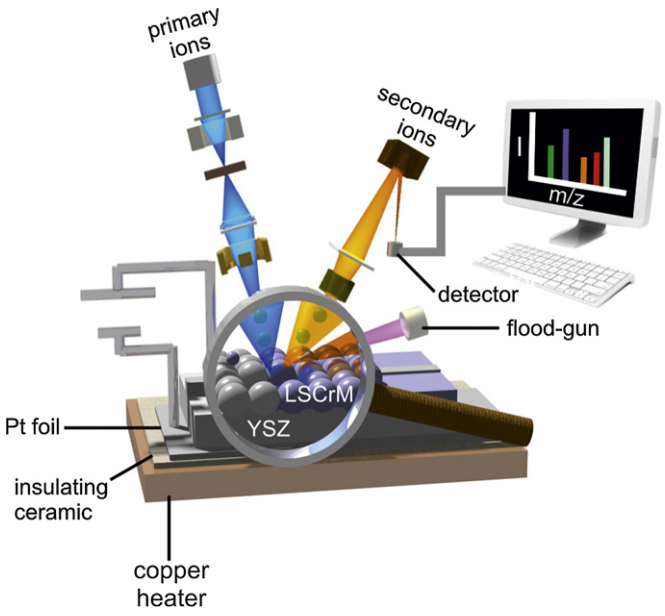

Fig. 2. Sample arrangement and measurement setup for in situ ToF-SIMS experiments. SIMS secondary ion images are collected on the surface at the interface between LSCrM and YSZ.

15 min and 60 min, and potentials in the range of −1.75 V to −2.0 V in cathodic and +1.5 V to +1.75 V in anodic direction were applied at temperatures between 600 °C and 800 °C.

For in situ characterisation the samples were heated up to 550 °C inside of the SIMS chamber. The essential elements of the measurement setup are presented in Fig. 2. For the heating and polarisation experiments a standard heating/cooling SIMS sample holder from IONToF company (Münster, Germany) was modified. Two additional electrical contacts were added to the sample holder for the polarisation. First, annealing experiments were performed. The sample was heated up for a period of 15 min–30 min at 550 °C, cooled down to minimise the background in the SIMS spectra and to quench the chemical state of the sample. Due to the high background intensity of thermally emitted ions from the sample surface and the residual gas it was not possible to perform SIMS measurements directly during the heating period. We therefore cooled the sample down rapidly and conducted the measurements at temperatures under 200 °C. The cooling rate was about 350 °C per 10 min, which quenched the samples quickly enough. The diffusion coefficient of a species must be higher than 10^{-17} cm^2 s^{-1} for a mean square displacement of at least 1 nm within this time. In the literature no low temperature diffusion coefficients are available. Taking into account high temperature data, the diffusion coefficients of all cationic species should definitely be lower than 10^{-20} cm^2 s^{-1}at 550 °C [31]. After surface analysis, the sample was heated up again, and the procedure was repeated typically three times for every sample until no further changes were detected.

For the polarisation experiments the electrode on the reverse side of the sample was contacted using platinum foil. The front contact on the LSCrM surface was made by a circle of conducting silver paste, placed about 2 mm away from the YSZ–LSCrM interface, and connected to a platinum wire. Prior to the polarisation experiment all samples were annealed in the SIMS chamber for 1.5 h until no further changes of the elemental distribution were observed. After every polarisation step the sample was cooled down in the same way as during the annealing experiments before starting ToF-SIMS analysis. Electrochemical polarisation was performed for different times between 20 and 30 min and potentials in the range of−1.5 V to −3.5 V in cathodic and +1.0 V to +2.8 V in anodic

direction at 550 °C. The polarisation voltage was supplied by a Keithley 2400 SourceMeter. Cathodic and anodic polarisation experiments were performed at two different oxygen partial pressures of approx. 1×10^{-9} mbar and 1×10^{-6} mbar. As the applied voltage would have disrupted the SIMS analysis, the electric polarisation was interrupted for a few minutes in order to record the secondary ion (SI) image. This interruption led to an unavoidable disturbance of the established stationary state. But as the establishment of the stationary state required more than 30 min at 550 °C, we assume that the short interruption at lower temperature did not cause a marked change of the surface state. Therefore, the measurements can only be regarded as "quasi in situ", but with the great advantage compared to ex situ polarisation that exactly the same small electrode area can be examined repeatedly, as the sample and the sample holder do not have to be moved for the polarisation experiments. In addition, surface contamination by exposure of the sample to ambient air was avoided. Since no transfer to the SIMS chamber was needed, re-heating followed by the next polarisation step could be started immediately after the uptake of the SI image, and therefore no significant relaxation took place.

Each experiment (ex situ/in situ annealing and polarisation) was repeated four times with different samples.

3.2. ToF-SIMS

In ToF-SIMS the secondary ions are differentiated by the time they need to pass the analyser after ionisation by bismuth primary ions and acceleration towards the analyser with a constant voltage of 2 keV. The lightest ion, hydrogen, reaches the detector first, as the flight time increases with the mass of the ions. Using the raster mode, SIMS images can be constructed and can directly be interpreted as concentration maps. Each image represents the spatial distribution of a particular ion, i.e. the spatial distribution of its "parent" neutral species (e.g. elements in the case of simple elemental ions, or molecules in the cases of molecular ions). If pixels are dark, comparatively few secondary ions were detected; if pixels are bright a comparatively high number of ions of the specified mass were detected. The secondary ions which form these images are chosen from the complete mass spectrum by selecting the corresponding mass range. If there are two SIs in the sample that have nearly the same mass (with respect to the mass resolution of the analyser) an unequivocal chemical interpretation is usually not possible. In some cases, the presence of a second isotope of an element helps to deconvolute the mass signal. Ion associates formed by two different ions from the sample or by reaction with the residual gas in the SIMS chamber may also cause mass interferences, if these associates have the same mass as another species in the sample.

Ions from surface regions that are located deeper or higher than the focus plane reach the detector later or earlier. In addition the ionisation process is influenced by the local electric field and geometrical effects. Thus, the intensity of the SI images is influenced from the surface roughness. To reduce these disturbances by the surface roughness, the SI image of each ion is normalised by division with the total ion image. In the total ion image all ions that have reached the detector contribute to the image. Therefore, regions located outside of the detector focus are darker than other regions. To a certain extent this normalisation also reduces the influence of the different ionisation probabilities of different materials, too. However, this correction is not sufficient if the differences in ionisation probability are high. Therefore, in the interpretation of SI images only concentration changes in the electrode material from one image to the following in each experimental session are compared with each other, but not with the concentration in the electrolyte area and vice versa. In addition to 2D surface analysis we collected 3D information on the bulk of the electrodes by using the depth profile mode. With the use of an additional sputter ion gun (caesium or oxygen ions) relatively rapid material erosion is achieved within the selected area. This material abrasion is frequently interrupted by analysis with the bismuth primary gun of the current surface in the sputter crater to obtain depth resolved concentration information. A sketch of the three different operation modes (mass spectra, secondary ion image and depth profile) in the SIMS analysis is depicted in Appendix 2.

For the SIMS measurements a TOF.SIMS 5-100 spectrometer (IonTOF, Münster, Germany) was used. The SIMS spectrometer was equipped with a bismuth cluster primary ion gun and with sputter guns for depth profiling (oxygen and caesium). In the present study only positive ions were considered. Images were created by bismuth primary ions, and in order to reduce noise the area of interest was usually scanned between 20 and 50 times for a single image. In the case of areas larger than $500 \times 500\ \mu m^2$ the number of superposed scans was reduced in order to shorten the time for the data collection.

In order to compare the surface images accurately, it is necessary to have comparable focus settings and analyser settings for each image. Due to the fact that the electrode has only a height of about 300 nm, both surfaces are within the same focus level of the ToF SIMS machine. Nevertheless the height difference of 300 nm causes a flight time difference. In consequence we receive two mass signals for each element which is on both surfaces. Elements from the bare YSZ surface have a slightly longer flight time and appear at higher masses. The mass signals can be resolved clearly and have no overlap. The reflectron voltage of the mass analyser was always optimised to the LSCrM surface to obtain comparable signal intensities. The image evaluation was done with the software Ion Image 4.1 (ION-ToF, Münster, Germany). For comparability, the image intensity level is the same for each species within each experimental row. The same intensity level was also chosen for all total ion images. For the elimination of possible topographical effects and variations in the primary ion current all images are normalised with respect to the total ion image.

Depth profiles were obtained by using oxygen sputter ions. For some depth profiles the sample surface was flooded with oxygen (1×10^{-6} mbar) to reduce the sample charging during the analysis process. The depth of the sputtered craters was either measured with a surface profiler (Alpha step iq, Tencor) or, in the event that the sputter crater was not found, calculated by using the known sputter yield from other measurements.

4. Results and discussion

4.1. Pre-annealing in air

As part of the preparation process the samples were annealed in a high temperature furnace directly after the deposition of the LSCrM films, thus establishing the right stoichiometry and crystal structure. In Fig. 3 SIMS images of the main elements of the sample surface are depicted. In the bottom left corner a part of the rectangular LSCrM electrode can be seen. According to the previously mentioned defect model the SI mass images show that already during the first annealing for 10 h at 1000 °C La and Sr started to diffuse on the bare YSZ surface. In contrast Cr, Mn and Zr did not spread. We cannot evaluate the spreading of Y, as it has the same mass as the SrH ion within the resolution limit of the mass analyser. The information on Sr is not hampered by this problem.

4.2. Annealing in the SIMS chamber at different $p(O_2)$

After the pre-annealing step in air a second annealing step in the SIMS chamber is performed at 550 °C. Annealing in the SIMS chamber is accompanied by transformation of the perovskite phase

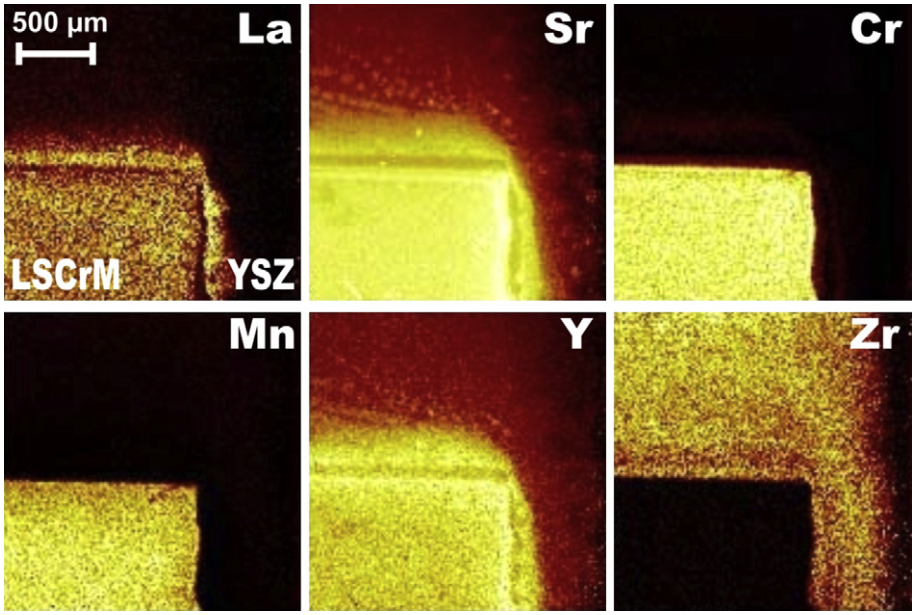

Fig. 3. Normalised secondary ion images of a LSCrM sample deposited on a YSZ single crystal by PLD after annealing for 10 h at 1000 °C in air. Field of view of each element picture is 2000 × 2000 µm^2. Only positive ions (singly charged) are included.

closer to the stoichiometric range leading to a decrease in the Sr and La surface concentration and diffusion of both elements in the bulk of the electrode and on the free YSZ surface. As can be seen from Fig. 4a we observe a depletion of strontium on LSCrM with increasing annealing time. In a further experiment the pressure in the SIMS chamber is increased from about 10^{-9} mbar to 10^{-6} mbar $p(O_2)$. In this case (see Fig. 4b) with increasing annealing time more and more Sr diffuses from the LSCrM film to the YSZ surface. At the boundary between the LSCrM and the YSZ we observe a rim and a strong depletion of Sr at the YSZ surface. Close to the interface with YSZ we find a rim with a higher Sr concentration than on the remaining LSCrM surface. This experiment shows that the Sr concentration on the LSCrM surface depends on the oxygen pressure in the gas phase.

In accordance with the defect model and in addition to the diffusion of Sr we find a diffusion of La and Mn from LSCrM to the YSZ surface. Cr shows enrichment at the interface between YSZ and LSCrM. In contrast to the re-distribution of Sr these processes are not influenced by the oxygen partial pressure in the chamber.

4.3. Electrochemical polarisation

By applying a cathodic potential we expect a segregation of Sr and La and maybe Mn and Cr from the electrode surface in the volume of the electrode and on the free YSZ surface.

By applying a cathodic potential of up to $V_{WC} = -2.0$ V to the LSCrM electrode no changes are observed at a pressure of 10^{-6} mbar within 30 min. At higher cathodic potentials we observe the suspected diffusion of Sr towards YSZ as can be seen in Fig. 5. In the case of anodic polarisation Sr diffuses back to the LSCrM. This process is well reproducible and we were able to switch several times between

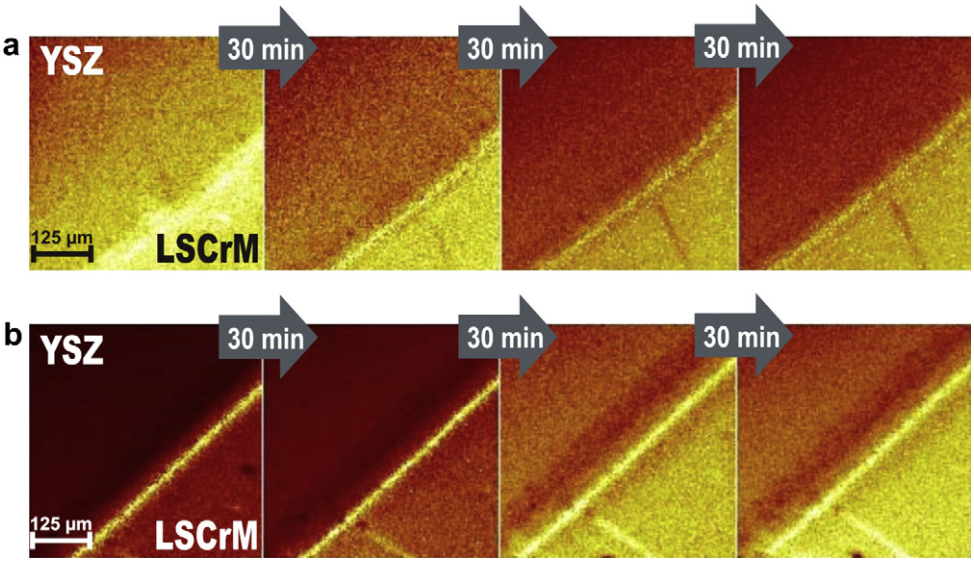

Fig. 4. SIMS secondary ion images of the strontium distribution of a LSCrM electrode surface during in-situ annealing experiments by ToF-SIMS at 550 °C and an oxygen pressure of a) 1 × 10^{-9} mbar and b) 1 × 10^{-6} mbar respectively. Between the imaging steps the samples were annealed for 30 min. Field of view of each picture is 500 × 500 µm^2. Positive ions have been regarded. All images of one mass were set to the same intensity level and normalised with the total ion image.

anodic and cathodic potential and to observe the same phenomena. La, Mn and Cr diffuse in the opposite direction of the Sr (conf. Fig. 6). Zr diffuses to the LSCrM with cathodic potential and backwards to the YSZ under anodic polarisation, as expected. If we polarise cathodically, we pump oxygen away from the YSZ surface. This should lead to a decomposition of the YSZ and the remaining cations spread over the LSCrM electrode due to a concentration gradient. Under anodic conditions oxygen is pumped towards the free YSZ surface and we find the reverse process.

At an oxygen pressure of 10^{-9} mbar the diffusion of the metal ions again shows different results. In general, the sample surface appears to be less stable against element re-distribution. The diffusion processes start to become visible in the SI images already at cathodic potentials higher than −1.5 V. Under cathodic polarisation we observe the suspected diffusion of Cr and Mn towards YSZ. Surprisingly the elements La and Sr diffuse back to the electrode (remember that we start with pre-annealed samples). In the case of anodic polarisation Cr and Mn diffuse back to the LSCrM whereas La and Sr diffuse towards the YSZ surface.

To obtain additional information on processes at even higher oxygen partial pressures we also performed polarisation experiments outside the SIMS chamber in a closed furnace with $p(O_2)$ control. The experiments were run in nitrogen (99.999%) atmosphere, and the oxygen partial pressure was slightly lower than 10^{-3} mbar. After applying a cathodic potential of −1.75 V to LSCrM for 60 min at 600 °C we observed that backdiffusion of Sr to the LSCrM surface had occurred. The La ions showed enrichment in a rim close to the interface on the LSCrM. The same was observed for Cr. These results are shown in Fig. 7. This experiment demonstrates that cation movement also occurs at higher oxygen partial pressures which are closer to applications.

4.4. Depth profiles

In addition to the surface imaging we measured depth profiles of LSCrM electrodes after different annealing times, see Fig. 8. The profile of a sample which was not annealed is shown in the upper row. The mass signals of the elements show a relatively sharp interface between LSCrM and YSZ. After annealing at $T = 1000$ °C for 100 h a transition region of approx. two μm thickness is detected where interdiffusion took place, as can be seen in the lower row of Fig. 8. In addition to the depth profiles on the electrode area, we also measured depth profiles on the bare YSZ area close to the electrode interface. Exemplary depth profiles are depicted in Appendix 3 and 4. The metals that can be found in the mass images on the YSZ were diffusing with time into the YSZ. Before starting the polarisation experiments we found the cations Sr, Mn, La and Cr only within 10 nm distance of the surface. After the polarisation experiments the diffusion profiles of Sr, Cr, Mn are much more extended. Whereas the diffusion length of Sr is about 300 nm, there is nearly no enrichment respectively diffusion of La. In order to determine the diffusion coefficients we used the equation for diffusion into a semi-infinite medium as solution for Fick's second law of diffusion [32]. For both La and Sr we obtain diffusion coefficients of about $D \approx 10^{-18}$ cm^2 s^{-1} which are roughly one order of magnitude higher than the data reported by Kilo et al. [30] in the range of 10^{-19} and 10^{-20} cm^2 s^{-1} for Sr and La, respectively. We determine the diffusion coefficient of Mn as $D(\mathrm{Mn}) \approx 10^{-20}$ cm^2 s^{-1} which is lower than the diffusion coefficient of Sr and La and still in agreement with values reported by Kilo et al. Due to the fact, that all of the literature values originate from high temperature experiments in slightly different YSZ compositions, we expect a higher deviation for the calculated values of the diffusion coefficients.

4.5. General discussion

With in situ SIMS we observed significant re-distribution (segregation) processes of cations from the electrode surface into the volume of the perovskite and towards the solid electrolyte and vice versa depending on the experimental parameters.

Naturally, the degradation of fuel cell components is mostly monitored macroscopically and in situ by electrochemical techniques (e.g. impedance spectroscopy [33]). Due to the intrinsic difficulty of combining electrochemical experiments at high temperature and atmospheric pressure with in situ spectroscopic and/or microscopic analysis, only a few combined studies exist to date. With improving experimental methods, their number is currently increasing, but still most chemical information on materials degradation under operation stems from post mortem analysis.

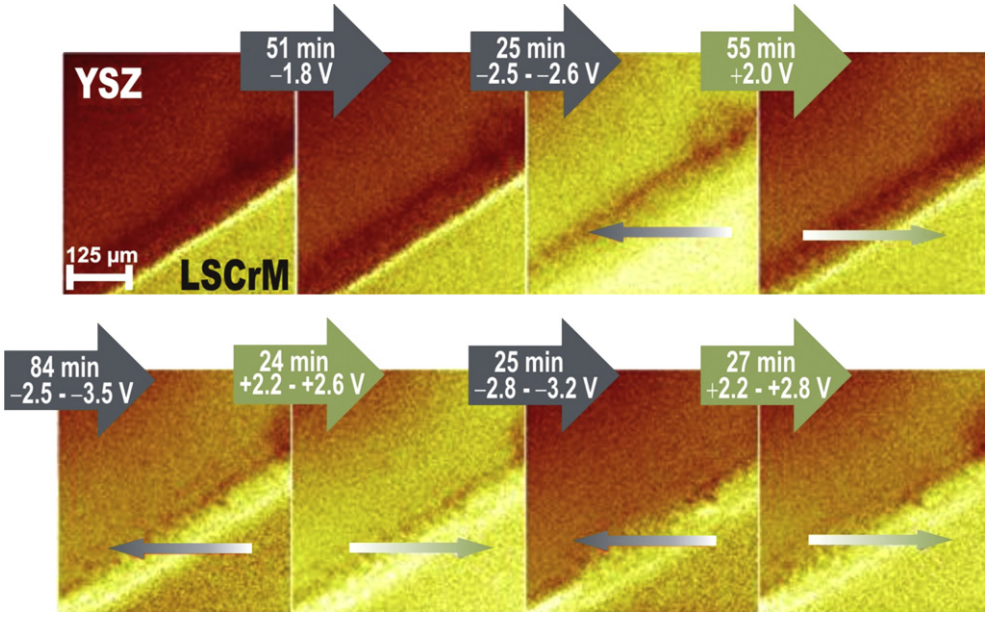

Fig. 5. SIMS secondary ion images of the strontium distribution during in-situ polarisation of a LSCrM sample deposited on YSZ (after annealing for 10 h at 1000 °C in air). The images were taken after polarisation at 550 °C and at an oxygen pressure around 1×10^{-6} mbar for different times and potentials which are noted in the pictures. Field of view of each element picture is 500 × 500 μm^2. Only positive ions have been regarded. All images of one mass were set to the same intensity level and normalised with the total ion image.

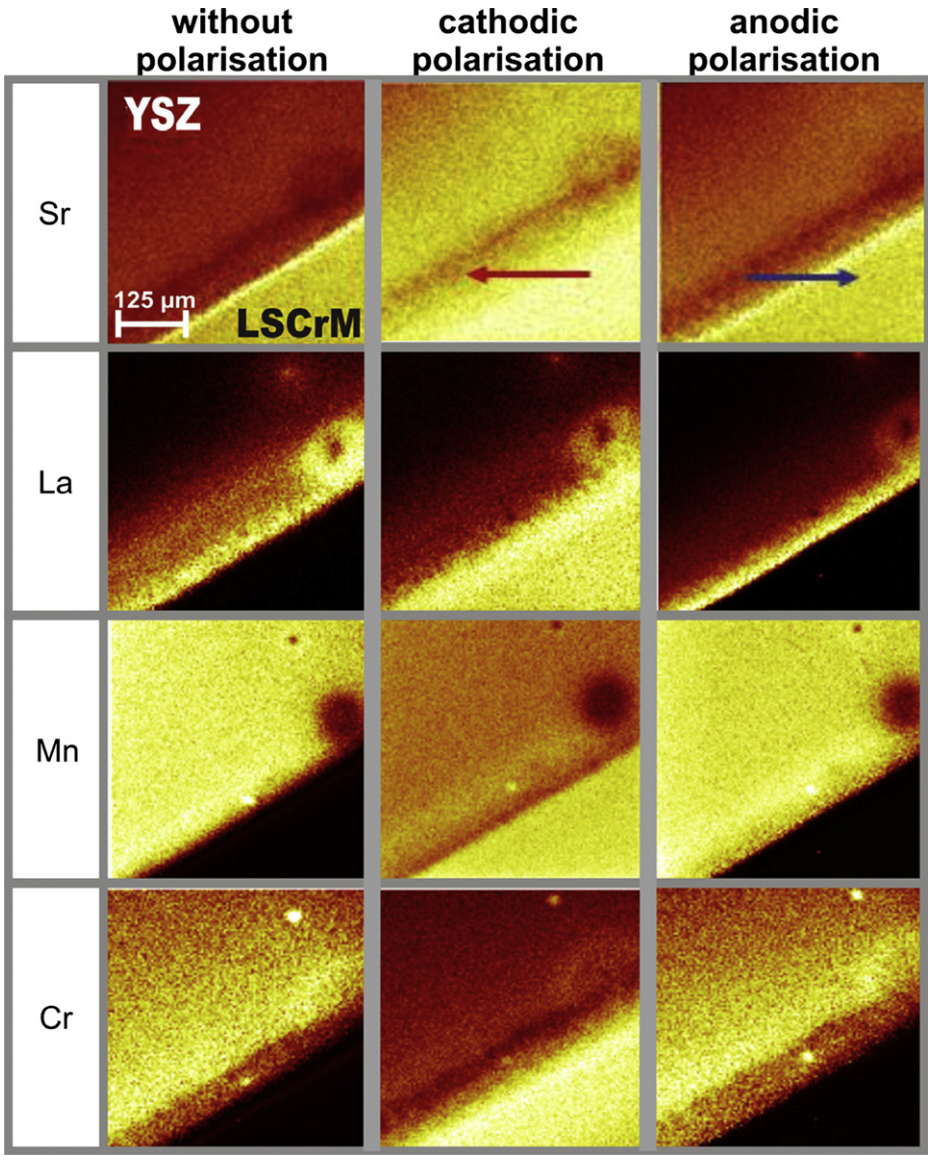

Fig. 6. SIMS secondary ion images of the different elements during in-situ polarisation of a LSCrM electrode deposited on YSZ (after annealing for 10 h at 1000 °C in air). The images were taken after polarisation at 550 °C and at an oxygen pressure around 1×10^{-6} mbar for different times and potentials. Field of view of each element image is $500 \times 500\ \mu m^2$. Only positive ions have been regarded. All images of one mass were set to the same intensity level and normalised with the total ion image.

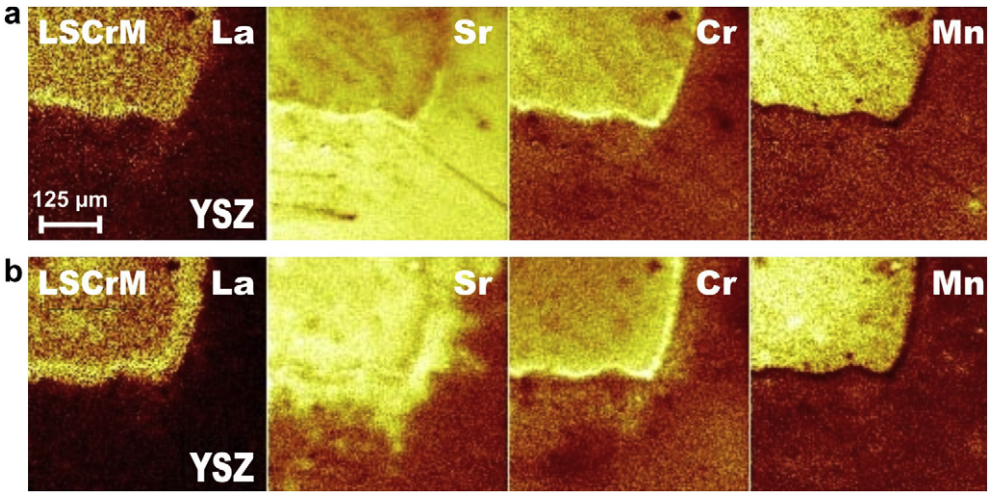

Fig. 7. SIMS secondary ion images of a LSCrM electrode deposited on YSZ after annealing for 10 h at 1000 °C in air a) before and b) after cathodic polarisation for 60 min at 600 °C and −1.75 V in N_2-atmosphere. Field of view of each element picture is $500 \times 500\ \mu m^2$. Only positive ions have been regarded.

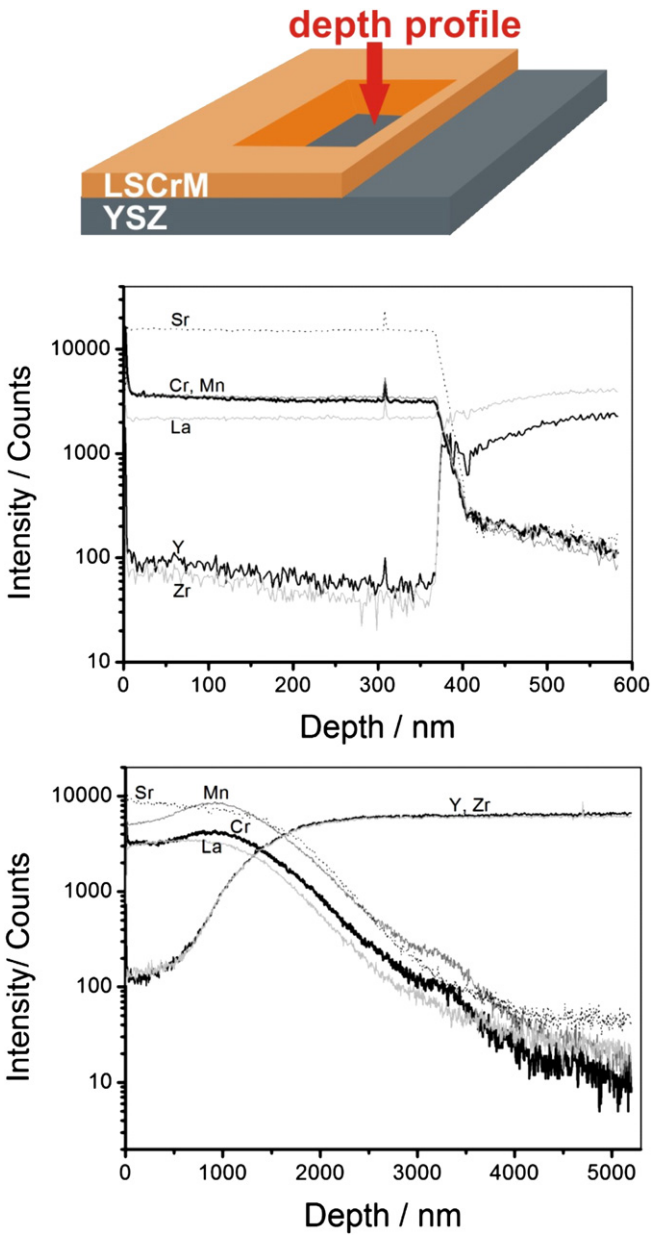

Fig. 8. Depth profile of a LSCrM sample deposited on a YSZ single crystal by PLD before (middle) and after annealing (bottom) for 100 h at 1000 °C in air together with a schematic sketch of the analysis position on the sample. Oxygen ions are used as sputtering ions, and positive ions have been regarded.

The consequences of surface segregation processes are not immediately obvious, and they may cause better or worse electrode kinetics. Interfacial reactions at the three phase boundary may become kinetically inhibited if blocking components from the electrode are transported on the electrode and towards the free YSZ surface. Alternatively, electronically and/or catalytically active components may accelerate electrode reactions by producing an extended three phase boundary on the free YSZ surface. In particular, Mn or Cr ions might act as catalytic centres on the YSZ surface. In fact, it was shown by Boukamp et al. that Fe-doping of YSZ enhances the oxygen exchange kinetics [34].

Several authors have reported a Sr surface segregation during the preparation of LSM electrodes. Decorse et al. [35] were the first who demonstrated a higher Sr surface concentration relative to the bulk composition in $La_{1-x}Sr_xMnO_{3\pm\delta}$ electrodes indicating SrO surface segregation. A segregation of Sr onto the electrode surface upon in situ heating under UHV conditions at 600 °C was reported by Wu et al. [36]. Wang and Jiang [37] were the first who proposed a modified defect model considering the segregation of Sr out of the lattice onto the electrode surface under anodic polarisation and vice versa under cathodic polarisation. In line with these results, the activation after cathodic polarisation was explained by removal of inhibiting SrO species from the electrode surface. But so far a direct evidence for these surface composition changes induced by electrochemical polarisation is still missing. A first ex situ investigation of potential driven segregation was performed by Caillol at al. [38] with X-ray photoelectron spectroscopy. The authors observed Sr enrichment on the surface of typical porous LSM-electrodes printed on YSZ at high temperature and low oxygen partial pressure during cathodic polarisation. They proved that the enrichment effect depends on the oxygen partial pressure, i.e. it takes place at low oxygen partial pressures, high temperatures and under cathodic polarisation. The enrichment could be reversed during annealing at intermediate temperature.

In accordance with the literature we also found Sr enrichment of the electrode surface after the preparation process. The composition changes during plain thermal annealing of the samples in the SIMS chamber can be explained thermodynamically. The oxygen partial pressure in the SIMS chamber was definitely lower than in the high temperature furnace where the samples were annealed before, and the samples equilibrate under the given environment. Thus, the surface state after about 90 min equilibration time represents the thermodynamically stable state at reduced $p(O_2)$. As predicted by the defect model we find typical Sr and La surface segregation at an oxygen partial pressure of 10^{-6} mbar at the annealing temperature of 550 °C. At lower oxygen partial pressure (10^{-9} mbar) surprisingly back-diffusion is observed. We cannot explain this behaviour now as it is contrary to the accepted defect model.

Cathodic polarisation is equivalent to reduction of the oxygen partial pressure (activity) at the electrode interface. This causes the re-distribution of the cations towards a new thermodynamic state, which – driven by the applied external force – represents a stationary state rather than equilibrium, once the partial pressure in the gas phase is not identical.

In agreement with the defect model the in situ SIMS experiments at an oxygen partial pressure of 10^{-6} mbar and under cathodic polarisation confirm the segregation of Sr onto the YSZ surface and in the volume of the electrode and vice versa by applying an anodic potential. Again in the case of the in situ polarisation experiments at lower oxygen partial pressure (10^{-9} mbar) the re-distribution behaviour of Sr is in the opposite direction and cannot be explained by the thermodynamic defect model.

An experiment under real operation conditions was reported by Backhaus-Ricoult et al. They studied the migration of Mn in $(La_{0.85}Sr_{0.15})Mn_{1.05}O_3$/3YSZ composite electrodes in a hydrogen/air atmosphere under cathodic polarisation, by using transmission electron microscopy (TEM) and electron energy loss spectroscopy (EELS) [39]. After operation of the SOFC cathode they find an enrichment of Mn at the cathode three phase boundary between YSZ, LSM and air. Moreover, Backhaus-Ricoult et al. [28] detected reversible polarisation induced redistribution of Mn on the electrolyte surface by spatially resolving ESCA. At sufficiently strong cathodic polarisation at voltages of −1.4 V and oxygen partial pressures of 10^{-6} mbar Mn^{2+} ions spread rapidly out of the electrode and diffuse under anodic potential back to it.

In our SIMS study we observe this only at low oxygen partial pressure of about 10^{-9} mbar, whereas at 10^{-6} mbar the reverse direction of Mn transport is monitored both during cathodic and anodic polarisation. The mechanism for the segregation of Mn ions out of the YSZ surface and into the perovskite lattice under cathodic polarisation is identical to the Sr segregation with the difference

that the cation mobility in the case of Sr(II) and La(III) is higher and therefore the diffusion of Sr should be more distinctive. Surprisingly, in the case of Mn segregation the behaviour at lower oxygen partial pressure (10^{-9} mbar) is in accordance with the defect model whereas the segregation at higher oxygen partial pressure (10^{-9} mbar) is inconsistent with the defect model. To our knowledge there exist no studies on the thermodynamic stability of the LSCrM phase. Backhaus-Ricoult et al. [28] present a stability diagram of LSM and manganese oxides as a function of temperature, oxygen partial pressure and applied electric potential. Due to the partial substitution of manganese with chromium in LSCrM, the absolute values in this stability diagram will not be valid, but we expect a comparable trend for this phase. Therefore, with increasing temperature and cathodic polarisation we expect to leave the phase field of the homogeneous phase and to enter the MnO phase. Backhaus-Ricoult et al. assume that the most pronounced effects occur in this region which is reached with the temperature of 550 °C in the SIMS chamber and a cathodic polarisation of approximately −2.0 V. This is in accordance with our observations that significant ion movement occurs only at cathodic voltages higher than −1.75 V. During cathodic polarisation the perovskite is reduced which causes removal of oxygen from the lattice. For charge compensation on the one hand manganese and/or chromium are reduced and on the other hand cation vacancies can be generated. This would be in accord with the observation that chromium and manganese diffuse out of the material during cathodic polarisation at low oxygen partial pressure of 10^{-9} mbar. During cathodic polarisation at higher oxygen pressure of 10^{-6} mbar both ions (Cr, Mn) diffuse in the reverse direction, thus, under these conditions the oxide phase seems to be stable.

In Figs. 9 and 10 we summarise the different observations during in situ annealing and polarisation at different oxygen partial pressure. As a thermodynamic model of LSCrM is yet missing, we cannot proof the mechanism based on the proposed defect model.

Taking into account the depicted depth profiles, we must keep in mind that diffusion of the metals of the LSCrM into the YSZ solid electrolyte takes place at every time. In comparison to the observed surface processes these bulk processes are slow. Surface diffusion coefficients are usually several magnitudes higher than bulk diffusion coefficients. Therefore we can neglect in first approximation the bulk diffusion processes of the cations. Nevertheless they are still running during the experiments and leads to the effect that we have a continuous loss of Sr, Cr, Mn, and La from the electrode into the bulk. In consequence the polarisation experiments can only be repeated several times.

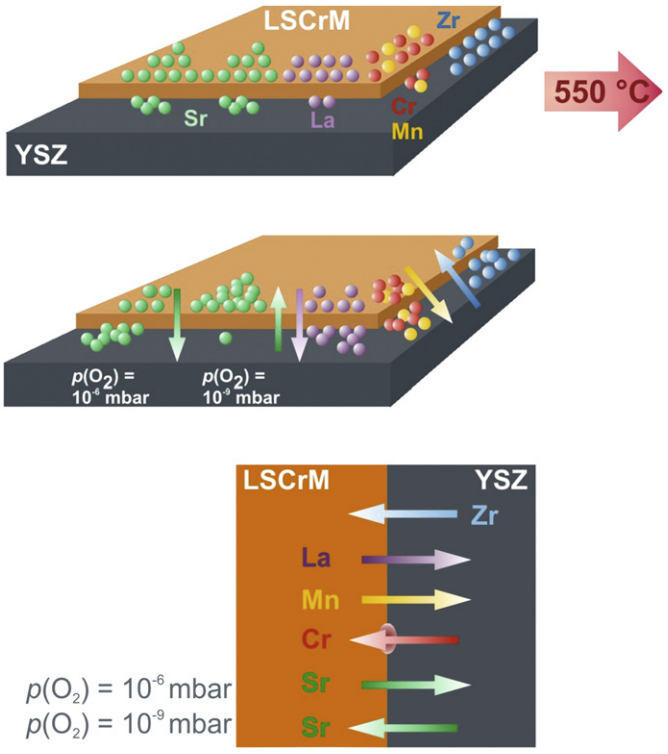

Fig. 10. Summary of the results on ion re-distribution in the LSCrM/YSZ electrode system during in situ annealing experiments at oxygen partial pressures of 10^{-6} mbar and 10^{-9} mbar. Strontium is the only ion showing different re-distribution at different oxygen partial pressure.

Our results prove that electrochemical experiments inside of a SIMS spectrometer can offer valuable information on the behaviour of electrodes under different experimental conditions. The major advantage of this technique is its high lateral resolution (up to 100 nm) and detection sensitivity (parts per billion). Very small

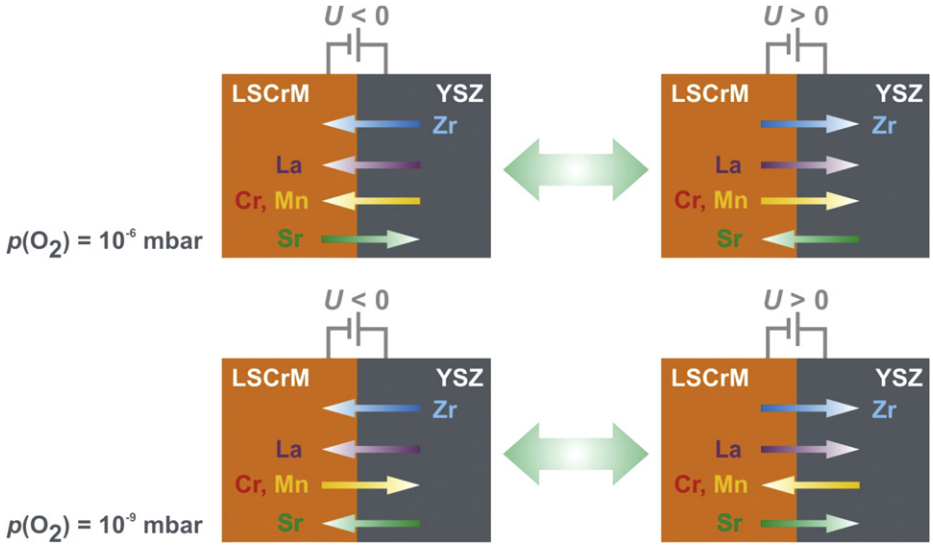

Fig. 9. Summary of the results on the ion re-distribution in the LSCrM/YSZ electrode system during in situ polarisation experiments at oxygen partial pressures of 10^{-6} mbar and 10^{-9} mbar. On the left side the re-distribution during cathodic and on the right side during anodic polarisation is summarised. We were able to switch several times the voltage direction, and the re-distribution is reversible within a few cycles. The upper part of the image depicts the situation at the higher, and the lower part depicts it at the lower oxygen partial pressure.

changes in composition on the electrode can be detected. Static SIMS is highly surface sensitive, and in addition, we can collect three-dimensional information in small volumes (about 100 μm × 100 μm × 10 μm) by measuring depth profiles. In performing the heating and polarisation experiments inside of the spectrometer we avoid contamination of the sample surface by e.g. the adsorption of CO_2 or water from the atmosphere and the formation of carbonates or hydroxides. Nevertheless, the approach has also some disadvantages: The samples are mounted on a heating stage with a maximum surface temperature of 600 °C. As a function of the thermal conductivity of the material and the pressure in the vacuum chamber, the surface temperature can be up to 50 K lower than the heater temperature. Thus, the samples should be very thin in order not to get large temperature gradients. For high quality SIMS analysis the samples should be as smooth as possible, in order to avoid a broadening of the mass signals. In contrast to XPS measurements it is not possible to obtain information on the chemical, i.e. the oxidation state. Finally, quantification requires a standard with the same matrix, as the ionisation probability depends strongly on the surrounding matrix. Finally, local differences in the microstructure and the interface properties may lead to differences in the segregation behaviour, which may explain the observed differences of the results from the simple thermodynamic expectation. Anyhow, the experimental approach is valuable in detecting electrochemically driven surface changes.

5. Conclusions

It was possible to perform high temperature electrochemical polarisation experiments inside a SIMS UHV analysis chamber. For the electrode system LSCrM/YSZ we demonstrated that already after short polarisation and annealing times diffusion processes take place at the surface, leading to a redistribution of the major chemical components. These surface diffusion and redistribution processes were partly reversible, but also led to irreversible changes which depend on the experimental parameters temperature, polarisation voltage and oxygen partial pressure. In the chosen system Sr showed the most pronounced re-distribution and appears to be particularly mobile. A defect model is proposed for the explanation of the observed phenomena. We are conscious of the fact that our experimental conditions pressure and voltage are different than the conditions in real solid oxide fuel cells. Nevertheless with our conditions we are simulating a fast ageing of the fuel cells under real operation conditions. Sooner or later the real systems should show degradation effects.

Acknowledgement

We thank Prof. A. Seubert (Analytical chemistry, University of Marburg) for the ICP-analysis of the LSCRM.

Appendix 1. XRD pattern of LSCrM

Fig. A.1. XRD pattern of the LSCrM thin film in black together with literature data [13], presented in red.

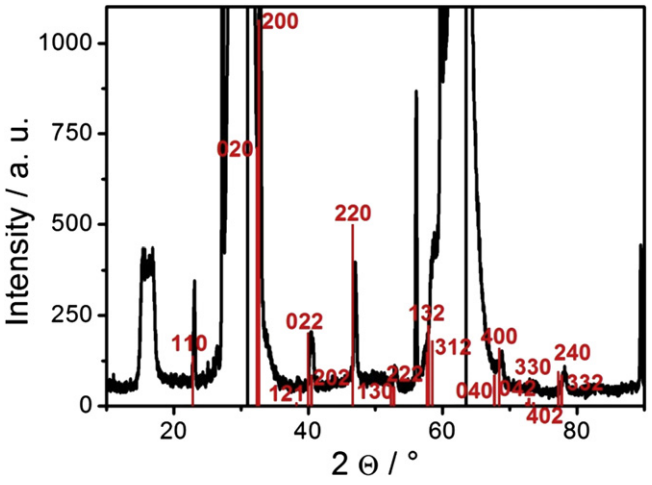

Appendix 2. Sketch of the ToF-SIMS experimental setup

Fig. A.2. Schematic sketch of the ToF-SIMS experiment. Bismuth ions are used as primary ions for analysis, and oxygen ions act as sputter ions for depth profiling. By rastering of the analysis gun over the sample surface a lateral resolved concentration map, the so called secondary ion image, is constructed from the local mass spectrum. During the depth profile mode images are recorded between the sputtering sequences to obtain concentration maps from various depths. In the so called depth profile the intensity of the single ions is represented as a function of the depth.

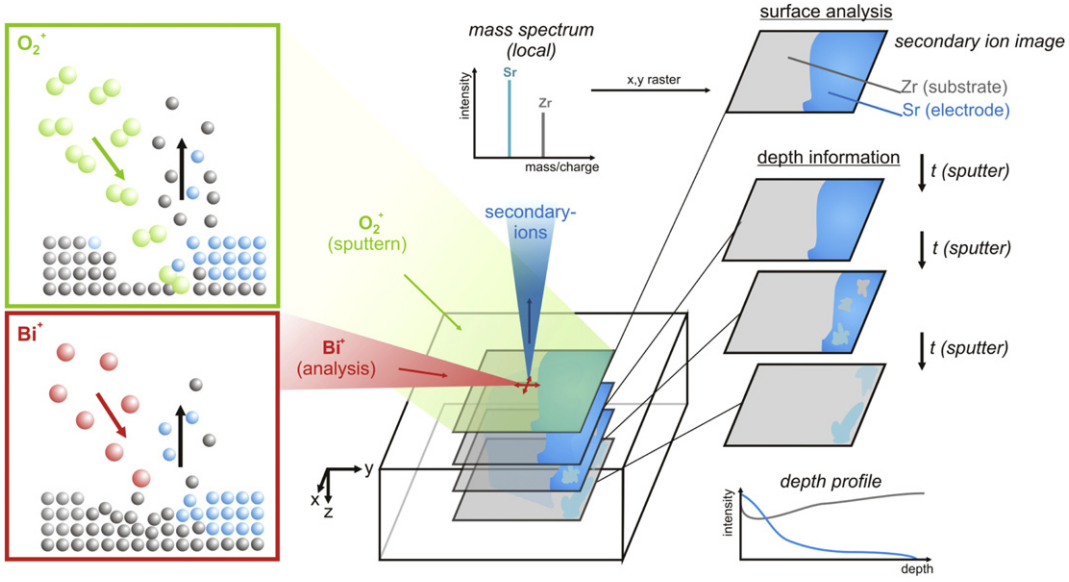

Appendix 3. Depth profile on the free electrode area

Fig. A.3. Depth profile of the strontium signal of the YSZ surface close to the LSCrM electrode and the corresponding fit for diffusion coefficient calculation as described in the text. Prior to SIMS measurement the sample was annealed for 10 h at 1000 °C in air.

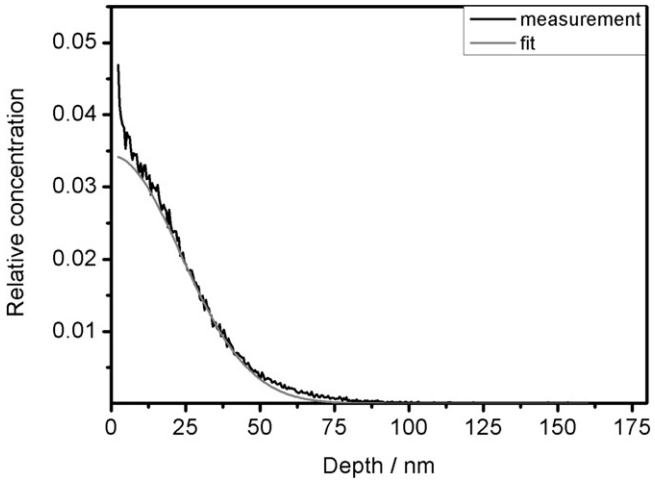

Appendix 4. Further depth profiles

Fig. A.4. Depth profiles of a LSCrM sample deposited on a YSZ single crystal by PLD after annealing for 10 h at 1000 °C in air a) before and b) after anodic polarisation at+1.75 V and 600 °C for 60 min in nitrogen. Oxygen ions are used as sputtering ions and positive ions have been regarded.

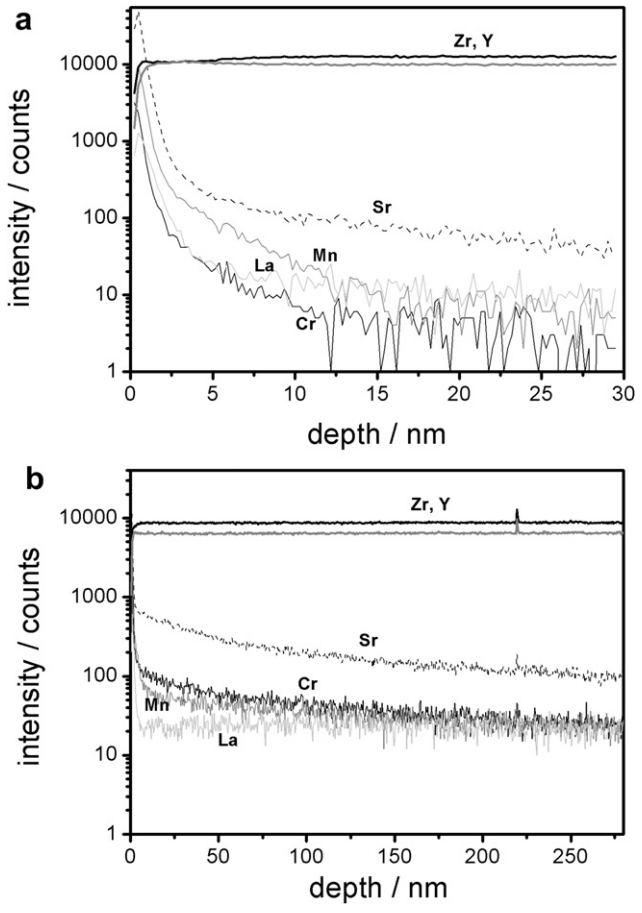

References

[1] J. Mizusaki, T. Saito, H. Tagawa, J. Electrochem. Soc. 143 (10) (1996) 3065–3073.
[2] E. Lay, G. Gauthier, S. Rosini, C. Savaniu, J.T.S. Irvine, Solid State Ionics 179 (2008) 1562–1566.
[3] S.B. Adler, Chem. Rev. 104 (2004) 4791–4843.
[4] H. Yokokawa, N. Sakai, T. Horita, K. Yamaji, M.E. Brito, H. Kishimoto, J. Alloys Comp. 452 (2008) 41–47.
[5] M. Backhaus-Ricoult, Solid State Sci. 10 (2008) 670–688.
[6] V. Stancovski, S. Sridhar, U.B. Pal, J. Electroceram. 3 (1999) 279–299.
[7] K. Kerman, B.-K. Lai, S. Ramanathan, J. Power Sourc. 196 (2011) 2608–2614.
[8] C. Zhang, M.E. Grass, A.H. McDaniel, S.C. DeCaluwe, F. El Gabaly, Z. Liu, K.F. McCarty, R.L. Farrow, M.A. Linne, Z. Hussain, G.S. Jackson, H. Bluhm, B.W. Eichhorn, Nat. Mater. 9 (2010) 944–949.
[9] A.-K. Huber, M. Falk, M. Rohnke, B. Luerßen, L. Gregoratti, D. Matteo, J. Janek, Phys. Chem. Chem. Phys. 14 (2012) 751–758.
[10] J. Janek, B. Luerssen, E. Mutoro, H. Fischer, S. Günther, Top. Catal. 44 (2007) 399–407.
[11] E. Mutoro, E.J. Crumlin, H. Pöpke, B. Luerssen, M. Amati, M.K. Abyaneh, M.D. Biegalski, H.M. Christen, L. Gregoratti, J. Janek, Y. Shao-Horn, J. Phys. Chem. Lett. 3 (2012) 40–44.
[12] Y.L. Liu, A. Hagen, R. Barfod, M. Chen, H.J. Wang, F.W. Poulsen, P.V. Hendriksen, Solid State Ionics (2009) 1298–1304.
[13] T. Horita, et al., Solid State Ionics 136–137 (2000) 897–904.
[14] A. Mitterdorfer, L.J. Gauckler, Solid State Ionics 111 (1998) 185–218.
[15] S. Fearn, J. Rossiny, J. Kilner, Solid State Ionics 179 (2008) 811–815.
[16] M. Martin, H. Schmalzried, Ber. Bunsen. Phys. Chem. 89 (1985) 124–130.
[17] M. Kubicek, A. Limbeck, T. Frömling, H. Hutter, J. Fleig, J. Electrochem. Soc. 158 (2011) B727–B734.
[18] J.S. Ping, J. Solid State Electrochem. 11 (2007) 93–102.
[19] J.H. Joo, R. Merkle, J. Maier, M. Kubicek, J. Januschewsky, J. Fleig, A. Oestereich, Z. Hlavathy, M. Hävecker, A. Knop-Gericke, R. Schlögl, Diffusions Fundam. 12 (2010) 67–68.
[20] B. Luerßen, J. Janek, S. Günther, M. Kiskinova, R. Imbihl, Phys. Chem. Chem. Phys. 4 (2002) 2673–2679.
[21] B. Luerßen, E. Mutoro, H. Fischer, S. Günther, R. Imbihl, J. Janek, Angew. Chem. Int. Ed. 45 (2006) 1473–1476.
[22] J. Janek, B. Luerßen, E. Mutoro, H. Fischer, S. Günther, Top. Catal. 44 (2007) 399–407.
[23] E. Mutoro, C. Hellwig, B. Luerssen, S. Günther, W.G. Bessler, J. Janek, Phys. Chem. Chem. Phys. 13 (2011) 12798–12807.
[24] I. Valov, B. Luerssen, E. Mutoro, L. Gregoratti, R.A. De Souza, S. Günther, A. Barinov, P. Dudin, M. Martin, J. Janek, Phys. Chem. Chem. Phys. 13 (2011) 3394–3410.
[25] T. Horita, K. Yamaji, M. Ishikawa, N. Sakai, H. Yokokawa, T. Kawada, T. Kato, J. Electrochem. Soc. 145 (1998) 3196–3202.
[26] A.K. Opitz, A. Schintlmeister, H. Hutter, J. Fleig, Phys. Chem. Chem. Phys. 12 (2010) 12734–12745.
[27] D.B. Bastidas, S.W. Tao, J.T.S. Irvine, J. Mater. Chem. 16 (2006) 1603–1605.
[28] A.K. Huber, M. Falk, M. Rohnke, B. Luerssen, L. Gregoratti, M. Amati, J. Janek, Phys. Chem. Chem. Phys. 14 (2012) 751–758.
[29] J. Mizusaki, N. Mori, H. Takai, Y. Yonemura, H. Minamiue, H. Tagawa, M. Dokiya, H. Inaba, K. Naraya, T. Sasamoto, T. Hashinoto, Solid State Ionics 129 (2009) 163–177.
[30] ICSD collection 98, FIZ Karlsruhe, Germany.
[31] M. Kilo, G. Borchardt, R.A. de Souza, E. Ivers-Tiffée, S. Weber, S. Scherrer, Electrochem. Soc. Proc. 99–13 (1999) 228–237.
[32] J. Crank, The Mathematics of Diffusion, Oxford University Press, Oxford, 1975, p. 13.
[33] M.C. Brant, L. Dessemond, Solid State Ionics 138 (2000) 1–17.
[34] B. Boukamp, B.V. Hassel, I. Vinke, K. de Vries, A. Burggraaf, Electrochim. Acta 38 (1993) 1817–1825.
[35] P. Decorse, G. Caboche, L.-C. Dufour, Solid State Ionics 77 (1999) 161.
[36] Q.-H. Wu, M. Liu, W. Jaegermann, Mater. Lett. 59 (2005) 1480.
[37] W. Wang, S.P. Jiang, Solid State Ionics 177 (2006) 1361.
[38] N. Caillol, M. Pijolat, E. Siebert, Appl. Surf. Sci. 253 (2007) 4641–4648.
[39] M. Backhaus-Ricoult, Solid State Ionics 177 (2006) 2195–2200.